Conference paper

Fei Xiu, Hao Lin, Ming Fang, Guofa Dong, Senpo Yip and Johnny C. Ho*

Fabrication and enhanced light-trapping properties of three-dimensional silicon nanostructures for photovoltaic applications

Abstract: In order to make photovoltaics an economically viable energy solution, next-generation solar cells with higher energy conversion efficiencies and lower costs are urgently desired. Among many possible solutions, three-dimensional (3D) silicon nanostructures with excellent light-trapping properties are one of the promising candidates and have recently attracted considerable attention for cost-effective photovoltaic applications. This is because their enhanced light-trapping characteristics and high carrier collection efficiencies can enable the use of cheaper and thinner silicon materials. In this review, recent developments in the controllable fabrication of 3D silicon nanostructures are summarized, followed by the investigation of optical properties on a number of different nanostructures, including nanowires, nanopillars, nanocones, nanopencils, and nanopyramids, etc. Even though nanostructures with radial p-n junction demonstrate excellent photon management properties and enhanced photo-carrier collection efficiencies, the photovoltaic performance of nanostructure-based solar cells is still significantly limited due to the high surface recombination effect, which is induced by high-density surface defects as well as the large surface area in high-aspect-ratio nanostructures. In this regard, various approaches in reducing the surface recombination are discussed and an overall geometrical consideration of both light-trapping and recombination effects to yield the best photovoltaic properties are emphasized.

Keywords: nanostructures, NMS-IX, photovoltaics, silicon.

***Corresponding author: Johnny C. Ho,** Department of Physics and Materials Science, City University of Hong Kong, 83 Tat Chee Avenue, Kowloon, Hong Kong SAR, China, e-mail: johnnyho@cityu.edu.hk
Fei Xiu and Senpo Yip: Department of Physics and Materials Science, City University of Hong Kong, 83 Tat Chee Avenue, Kowloon, Hong Kong SAR, China; and Shenzhen Research Institute, City University of Hong Kong, Shenzhen, China
Hao Lin, Ming Fang and Guofa Dong: Department of Physics and Materials Science, City University of Hong Kong, 83 Tat Chee Avenue, Kowloon, Hong Kong SAR, China
Johnny C. Ho: Shenzhen Research Institute, City University of Hong Kong, Shenzhen, China; and Centre for Functional Photonics (CFP), City University of Hong Kong, 83 Tat Chee Avenue, Kowloon, Hong Kong SAR, China

Article note: A collection of invited papers based on presentations at the 9th International Conference on Novel Materials and their Synthesis (NMS-IX) and the 23rd International Symposium on Fine Chemistry and Functional Polymers (FCFP-XXIII), Shanghai, China, 17–22 October 2013.

Introduction

Over the past decades, highly efficient solar cells have become one of the extensive research topics in various science and engineering disciplines [1–6] since solar energy is by far the most abundant renewable clean-energy resource. For example, among many renewable alternatives, solar energy can provide more energy in 1 h to the earth than all of the energy consumed by humans in 1 year [7]. Until now, crystalline silicon (Si) remains the major workhorse of photovoltaic (PV) materials because of its well-developed infrastructure in electronic and semiconductor industries. However, the large-scale implementation of crystalline Si solar cells is still not that economically attractive as a result of the high processing and materials costs, coming from the high-temperature fabrication

steps involved and the required thickness of silicon substrates for the effective absorption of solar spectrum due to its indirect bandgap of 1.1 eV. In order to maximize the development of Si PVs and make it an economically viable energy solution, it is necessary to further improve the energy conversion efficiency as well as to lower the material and manufacturing costs. In this regard, a new generation of highly efficient, low-cost PV materials and novel device structures has been recently developed to address the above issue [8–12]. In particular, an assortment of three-dimensional (3D) Si nanostructures has been fabricated with various processing techniques. These nanostructures are of the great interest for PV applications owing to the enhanced light trapping properties plus the high carrier collection efficiency by separating the path for light absorption and carrier collection, utilizing the radial core-shell p-n junction structure to increase the junction area [8, 13]. It has been reported that by controlling light at the nanometer scale using these nanostructures, a development of solar cells with efficiencies up to the range of 50–70 % can be reached theoretically, breaking the Shockley-Queisser limit [14]. At the same time, the material cost of these nanostructured PV devices can be significantly reduced due to the enhanced light absorption and thus employing less or inexpensive silicon substrates, without adding much to the processing cost [15]. While most studies show that the PV performance of nanostructured solar cells is greatly limited by the high carrier recombination rate caused by the high density surface or interface defects in nanostructures with the large surface area, in spite of the strong optical enhancement [9, 16–18]. To suppress this carrier recombination, it would be critical to take proper surface treatments, such as depositing appropriate surface passivation layers (e.g., silicon oxide and hydrogenated silicon nitride) [19–23]. Recently, Wang et al. [18] have found a chemical polishing etching (CPE) treatment as another effective way to reduce the surface recombination in high-aspect-ratio nanostructures. By decreasing the surface defects and controlling the final morphologies of the as-made structures with CPE, the solar cells fabricated with hierarchical structures exhibit the impressively high efficiency of 15.14 % [18]. Therefore, all these nanostructures demonstrate the technological potency of being promising candidates for the next generation solar cells with higher energy conversion efficiencies and lower costs.

In this report, we aim to provide a comprehensive review of recent progress on several major categories of Si nanostructures with excellent photon management properties for PV applications. These nanostructures include nanowires (NWs), nanopillars (NPs), nanorods (NRs), nanopencils (NPLs), nanopyramids (NPMs), nanocones (NCs) and nanodomes (NDMs), etc. We will begin and emphasize with a brief survey of recent developments in the fabrication techniques for various Si nanostructure formations. Then, optical properties of the aforementioned nanostructures will be investigated in details. Special attention will be paid to the different light trapping characteristics of these nanostructures, suggesting the appropriate geometrical and morphological design guidelines for the efficient light harvesting. Moreover, nanostructure-based PV applications will be discussed thoroughly followed by the novel approaches to reduce the surface recombination of carriers in the high-aspect-ratio nanostructures. All these would deliver an overall geometrical consideration of both light trapping and surface recombination effects in order to yield the best PV properties.

Fabrication approaches for the formation of three-dimensional silicon nanostructures

Controllable fabrication of 3D Si nanostructures is crucial for their light harvesting properties and corresponding PV applications. To control various geometrical and morphological parameters of the nanostructures, numerous methods including both “top-down” or “bottom-up” approaches have been developed, such as vapor-liquid-solid (VLS) growth, reactive ion etching (RIE), metal-assisted chemical etching (MacEtch) and so on.

Vapor-liquid-solid (VLS) growth

One of the most effective ways to achieve the bottom-up fabrication of Si nanowires can be done by the metal-catalyzed vapor-liquid-solid (VLS) growth technique [24]. In this approach, as shown in Fig. 1a, metal

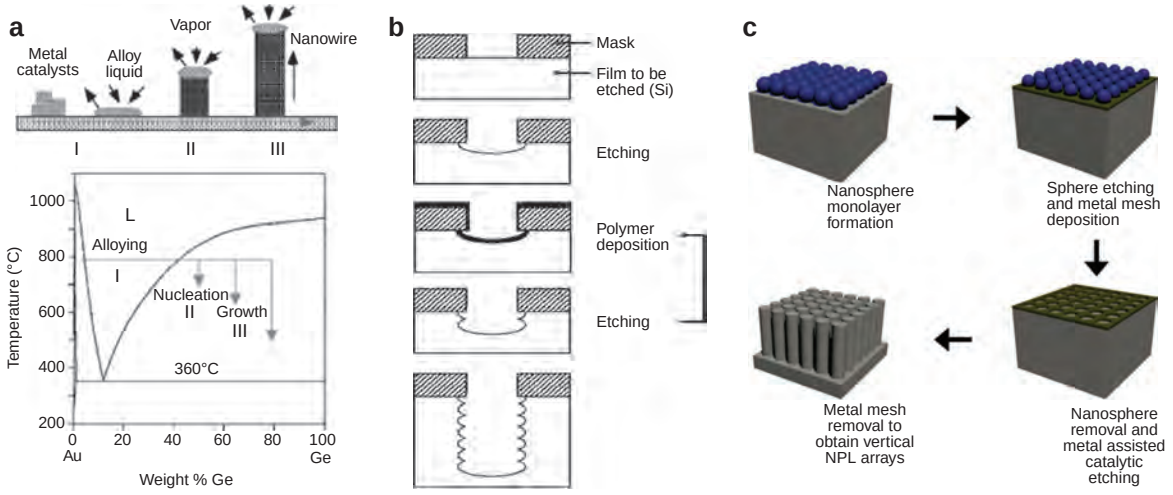

Fig. 1 Schematic illustration of (a) the VLS NW growth mechanism (top) and the conventional Au-Ge binary phase diagram to demonstrate the composition and phase evolution during the NW growth process (bottom), (b) individual steps in the deep reactive ion etching (DRIE) process and (c) the nanosphere lithography followed by the metal-assisted chemical etching (MacEtch) processes. Reproduced from Refs. [25, 53, 59] with permission from The American Chemical Society, The American Institute of Physics and The Royal Society of Chemistry.

nanoparticles (e.g., Au) can catalyze the growth of nanowires by forming a liquid metal droplet at an elevated temperature through which the growth atoms are transported to the crystallizing interface from the gas phase with silicon containing species [25]. This is known as the chemical vapor deposition (CVD) [26–28]. Specifically, silane (SiH_4) or tetrachlorosilane ($SiCl_4$) is usually used as the gas precursor providing Si constituents. Once the vaporized growth species reach the substrate surface that is covered with metal nanoparticles and the substrate temperature is held above the eutectic temperature of the Au-Si alloy, the liquid alloy droplet can be supersaturated with silicon atoms [29]. Then, Si NWs can be grown by the precipitation of Si from the catalytic alloys. Among several methods for realizing a forest of Si nanostructure, VLS technique is considered attractive owing to its process simplicity and potential scalability suitable for large-area device fabrication [30]. There have been several in-depth studies to fabricate radial p-n junction solar cells based on these VLS-grown NWs and their PV properties are investigated accordingly [16, 31, 32]. Meanwhile, for the VLS grown NWs, it is found that even the smallest concentration of catalytic Au atom can still reside as dopants or deep-level energy traps in Si, which would have a detriment influence on the properties of Si NWs [33]. The corresponding overall energy conversion efficiency of fabricated solar cells is then seriously limited by the carrier recombination within the depletion region or at the surface of VLS grown NWs due to this Au contamination. For instance, Gunawan et al. reported the fabrication and characterization of core-shell radial p-n junction Si NW solar cells, with the NWs synthesized by the VLS method using SiH_4 as a source gas while PH_3 and B_2H_6 as the gas-phase dopant precursors [16]. The short-circuit current density (Jsc) is improved which is attributed to the enhanced optical effects of low surface reflectance and light trapping in NWs within the device. However, the excessive Au residual trapped in the NWs as well as the excess surface recombination due to the increased NW surface area ultimately limit the minority carrier lifetime and cell performances in spite of the strong optical enhancement, indicating that the amount of metal catalyst incorporated in the VLS process has to be minimized.

In this regard, NWs produced by the non-catalytic growth mechanism seem to suit better for the PV applications as there is no involvement of metal impurities [33, 34]. Much progress has been made in the catalyst-free growth of semiconductor NWs achieved by various methods, including laser ablation [35], physical vapor deposition [36], chemical vapor deposition [37] and vapor phase epitaxy, etc. [38, 39]. Two main steps are typically reported in this non-catalytic growth [34]: (1) the nucleation of seed nanoparticles controlled by the

thermodynamic size limit and (2) the subsequent anisotropic NW growth without the catalyst. For example, the non-catalytic growth of Si NWs has been dominated by the oxide-assisted growth (OAG) approach in which evaporation and deposition of oxide vapor can form crystalline NWs with the amorphous oxide shells [40–42]. In this method, oxides, instead of metals, play an important role in inducing the nucleation and growth of NWs [43–45], thus allowing the large-quantity production of Si NWs free of metal impurities [41]. However, this technique requires the growth at high temperatures (>850 °C), which may restrict the practical implementation for scale-up processes. Furthermore, the control of structural defects, NW physical dimensions and in situ doping may not be as viable as in the metal-catalyzed CVD method [46]. In any case, Kim et al. introduced a non-catalytic CVD growth of single-crystalline Si NWs by nucleation of nanocrystalline seeds on the reactive oxide surface and subsequently achieved the anisotropic growth using the low-pressure CVD process at lower temperature (<650 °C) [46]. The NW diameter and doping level could be well controlled by adjusting the growth conditions, such as the growth temperature and ratio of precursor partial pressures.

Deep reactive ion etching

Another approach for realizing nanoscale vertical Si structures relies on the "top-down" manufacturing, namely high-aspect-ratio anisotropic etching of Si substrates. Deep reactive ion etching (DIRE) is regarded as a powerful method to fabricate vertical Si nanostructures among various "top-down" methods [47–50]. At present, the anisotropic DRIE of Si has already been a mature process technology which is used for creating 3D Si structures for various applications [51, 52]. As depicted in Fig. 1b, a typical DRIE process involves the use of high-density plasma and comprises a sequence of alternating steps (no more than a few seconds long) of Si etching and polymer deposition to protect the already-carved features from further lateral etching [53]. It is observed that as the cycles go on, the micromachining proceeds via a series of "bites" into the silicon and "scalloping" (or "ripple") morphology is easily to be formed on the sidewalls [51, 52]. When the feature size and scallop size become comparable, scalloping can become a serious problem for the nanostructure [49, 50]. In order to ensure smooth sidewalls at the nanoscale, as demonstrated by Fu et al., the process conditions of DRIE have to be well controlled to minimize the ripple effect and this can be achieved by optimizing the source power, bias power, gas flow rate, flow cycle time, substrate temperature, and chamber pressure [54]. They also illustrated an optimized DRIE process for the successful fabrication of large-area Si nanostructures, including nanopillars, nanowires and nanowalls with smooth sidewalls, emphasizing the great potential of DRIE for ultrasmall, large-area and 3D nanofabrication. Besides the ripple effect, RIE-related surface contamination and substrate displacement damage are also involved: (1) surface residues such as halocarbon films; (2) impurity implantation or penetration such as hydrogen diffusion; (3) lattice damage due to energetic ions or radiation while heat treatments can be utilized to anneal out this damage; (4) heavy-metal contamination including the reactor wall constituents diffusing readily into Si; (5) mobile ion contamination such as sodium from Teflon electrodes [55]. All these could subsequently leads to the limitation in PV applications due to the defect-rich surface and residual contamination on the fabricated structures.

Wet metal-assisted chemical etching

Recently, metal-assisted chemical etching (MacEtch) [15, 56–59], a wet but directional etching method, has attracted increasing attention as a simple and low-cost technique for fabricating various Si nanostructures. This technique can come with the ability to control various important parameters for NW based PV devices, including the NW diameter, length, orientation, cross-sectional shape, doping type and doping level, etc. Compared with dry etching processes, MacEtch is free of surface damage because there are no high-energy ions involved. MacEtch also does not induce metal contamination as happened in the VLS method since it takes place at room temperature and the metal catalyst cannot be incorporated in Si [15]. In addition, it is a more flexible technique and can be used to make higher surface-to-volume ratio structures [47, 60], while

VLS-based method can only be used to grow wires with circular cross-sections. Furthermore, MacEtch is scalable to the wafer scale easily with the lateral resolution as high as 10 nm through various metal patterning schemes such as the superionic solid state stamping [61], colloidal lithography [62, 63], electron beam lithography [64], or soft lithography [65]. For example, as given in Fig. 1c, we have attained the Si nanopillar (NP) arrays utilizing the colloidal or nanosphere lithography followed by the MacEtch process [59]. In brief, monodispersed polystyrene (PS) nanospheres were assembled into a close-pack monolayer on Si (100) substrates employing the Langmuir-Blodgett (LB) method. The substrates were then pre-treated with controlled oxygen plasma to result hydrophilic surfaces for the enabling of uniform nanosphere coating. The dimension and distance pitch of the spheres could be manipulated by the subsequent oxygen plasma etching. These obtained spheres were used as the mask and 1.5/20 nm thick Ti/Au metal mesh was thermally evaporated. As shown in Fig. 2a and e, Si NPs with the controllable diameter and periodicity could be realized via the MacEtch in HF/H_2O_2 solution.

More importantly, exploiting these NP templates, we have developed an anisotropic wet-chemistry only fabrication scheme for the formation of large-scale, low-cost, highly regular, single-crystalline and high aspect ratio Si nanostructures with different geometrical morphologies, ranging from nanopillar, nanorod, nanopencil and nanocone arrays for the efficient light trapping (Fig. 2b–d and f–h) [59]. In this work, once the NP templates were obtained, they were treated with a mixture of $AgNO_3$, HF, and HNO_3 or H_2O_2 for two functions. This chemical mixture would first lead to the selective deposition of Ag clusters at the NP tips and simultaneously perform Si etching. The subsequent removal of Ag clusters by HNO_3 washing gave truncated NP tips and this deposition/removal processes were repeated with multiple times to provide different morphological NP arrays with well-regulated chemical conditions. Notably, since Ag nanoclusters were observed to be preferentially formed around the rim of the tip, this indicated that Si atoms in the rim region are more reactive than those in the core region. This difference in the reactivity is mainly attributed to the different crystallinity of Si in different regions, where this rim edge has as well been observed in other material systems [66]. Therefore, the site-specific reactivity of Si is the key for this anisotropic etching. In addition, the etching kinetics could be tailored by varying the concentration and the components of the [$AgNO_3$ + HF + HNO_3] mixture to achieve different morphologies. Specifically, nanocones could be obtained by the addition of extra $AgNO_3$ to HF, in which the extra $AgNO_3$ speeded up the formation of Ag nanoclusters [59]. It is also noted that the use of the [$AgNO_3$ + HF + H_2O_2] system yielded nanorods with the dome head terminal, which was accredited to the existence of Ag(nanocluster)-catalyzed decomposition of H_2O_2 that changes the oxidation kinetics of H_2O_2. The detailed mechanistic processes are summarized in Fig. 3 for the fabrication of nanorods, nanopencils and nanocones, respectively.

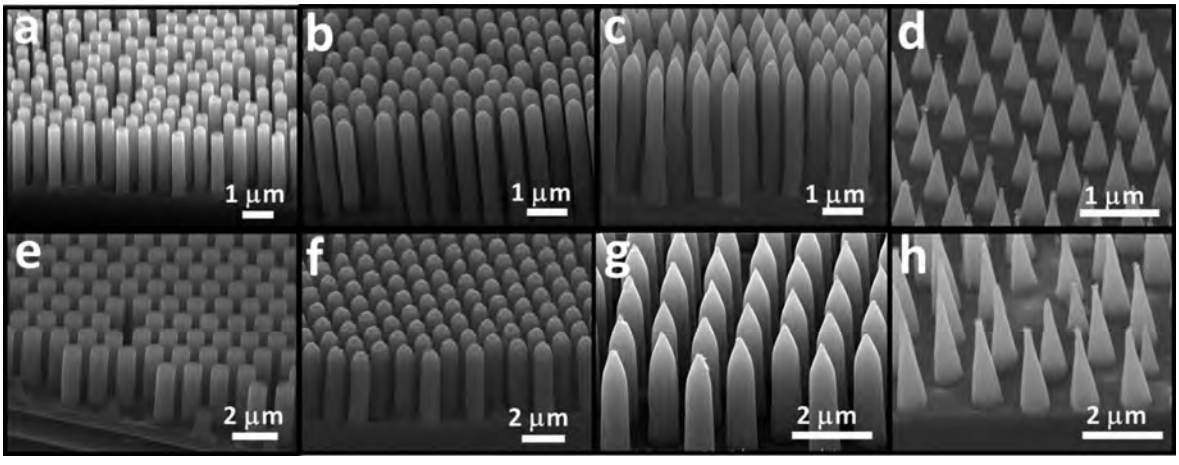

Fig. 2 SEM images of the fabricated high-aspect (a, e) nanopillar, (b, f) nanorod, (c, g) nanopencil, (d, h) nanocone arrays for the pitch of 0.6 and 1.27 μm, respectively, via the MacEtch processes. Reproduced from Ref. [59] with permission from The Royal Society of Chemistry.

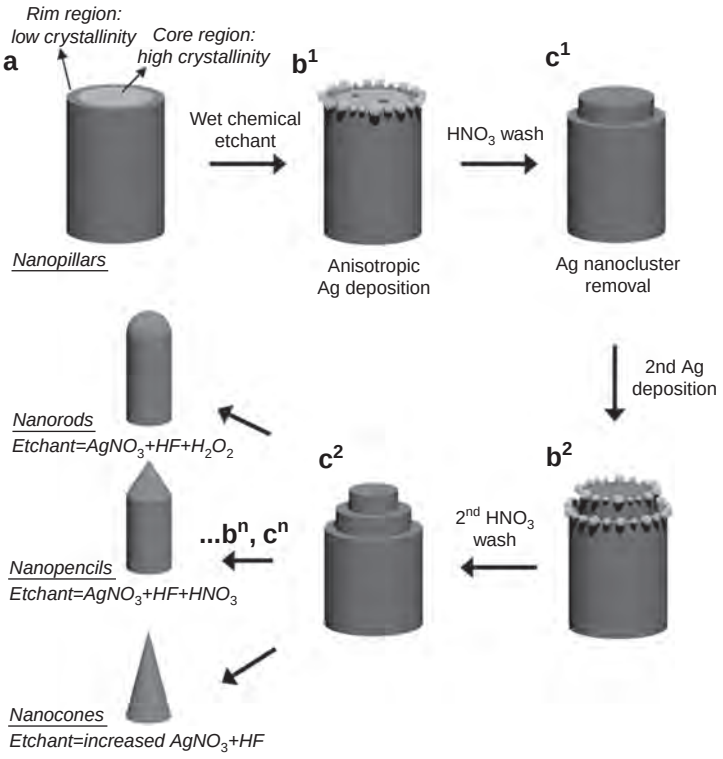

Fig. 3 Schematic illustration of the formation mechanism for various Si nanoarrays with different geometrical morphologies. Reproduced from Ref. [59] with permission from The Royal Society of Chemistry.

Light-trapping properties of various silicon nanostructures

Nanowires and nanopillars

The anti-reflection properties of silicon nanowire arrays (NWAs) have been extensively studied theoretically as well as experimentally [8, 58, 67]. As efficient absorber materials, NWAs can prolong the optical path length of the incident light by increasing the frequency of the reflected waves bouncing between wires, reducing the opportunity for the light to escape from the surface. By designing NWAs with different geometries (i.e., diameter, length and pitch), Garnett et al. have demonstrated the tunable light trapping properties with their NWAs [67]. Figure 4a gives the tilted cross-sectional SEM view of ordered silicon NWAs fabricated by the DRIE process [67]. The pitch and diameter of the nanowires are controlled by the diameter of mask (i.e., silica beads), while the length is determined by the etching time. Optical measurements are then performed on the Si substrates before and after the NW fabrication, which illustrate that NWAs yield the lower reflection property over the entire spectral range from 600 to 1100 nm as compared with the planar Si. Also, there is a red shift regarding the frequency of the transmitted light that is expected for a strong light-trapping effect. Obviously, tunable anti-reflection can be controlled by the length of NWs and longer NWAs exhibit the superior anti-reflection property due to an increase of the effective path length (Fig. 4b). On the other hand, a very low reflectivity (<2 %) has been realized in the 300–600 nm wavelength range in the case of 12 μm long Si wires, as demonstrated by Srivastava [59]. Si nanostructures with the very low reflectivity and correspondingly high absorption of visible (and infrared) light is named as black silicon. However, remarkable defect concentrations are existing on the surface of such Si NWs due to the fabrication processes. Combining with their relatively large surface area, the high surface recombination is resulted, which ultimately limits the corresponding energy conversion efficiency of nanotextured black Si solar cells [68, 69].

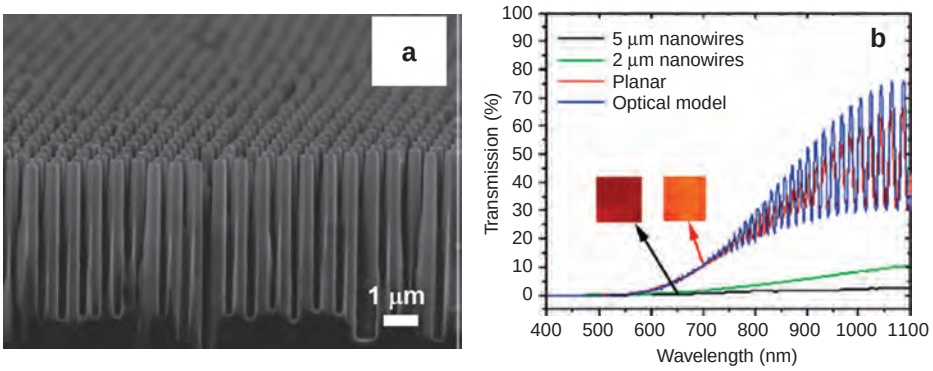

Fig. 4 (a) Tilted cross-sectional SEM image of an ordered silicon nanowire radial p-n junction array solar cell. (b) Transmission spectra of thin silicon window structures with 2 μm (green) and 5 μm (black) long nanowire and with planar surface (red), with the blue curve corresponding to an optical model for a 7.5 μm thin silicon window. Reproduced from Ref. [67] with permission from The American Chemical Society.

Compared with NWAs, Si NPs are becoming more attractive because of their unique optical properties, especially for their less surface recombination due to the relatively smaller surface area, which make them a potential candidate for the PV applications [70, 71]. Yi et al. reported the fabrication of NP-based Si solar cells with tunable pillar diameters and height [72]. They demonstrated that the lower reflectance of these solar cells is obtained which can be attributed to the enhanced light trapping and effective absorption of the pillar structure, in contrast to the conventional pyramid surface texturized solar cell structures. Optical and PV characteristics of these cells such as the reflectivity, photovoltaic conversion efficiency (PCE), external quantum efficiency (EQE) and so on are greatly influenced by the average diameter and height of nanopillar arrays. Notably, the NPs with small diameters and large height can suppress the reflection, but less advantageous for PV performances since they inherently come with the large surface area for the significant surface recombination and a greater number of lattice defects. In their work, the lowest reflectivity was achieved for Si NPs of 200 nm average diameter and 1.5 μm height, where the reflectivity was measured below 5 % for the wavelength range of 400–1000 nm, but the best performed solar cell made with Si NPs of 600 nm average diameter and 1.5 μm height (PCE ~14.83 %) [72]. More importantly, although all these Si NWAs and NPs have presented the impressive light trapping characteristics, the large-scale deployment of these structures is needed for the practical implementation of solar cells. In this regard, Pudasaini et al. reported that highly ordered wafer-scale Si NP arrays were successfully fabricated by the MacEtch process in combination with the nanosphere lithography [9]. The fabricated NPs were then incorporated into the Si/organic polymer hybrid solar cell devices, with the aim to utilize these semiconductor nanostructures as an efficient electron accepting phase for the low-cost hybrid PVs. Figure 5a demonstrates SEM images of the vertically aligned Si NP arrays with the hexagonal order [9]. The pitch of NP arrays is 650 nm and Si NPs with different heights are fabricated by varying the Si etching time. Reflectivity spectra presented in Fig. 5b show that the stronger anti-reflection property could be observed as the height of NP increases. Further investigation in the effect of NP height on the corresponding PV performances was carried out and found that the measured external quantum efficiency (EQE) of the Si NP/PEDOT:PSS solar cells improves with the increase in the NP height up to 0.4 μm due to the light trapping effects. Beyond 0.4 μm height, the EQE decreases drastically with the increase in the NP height, despite of their effective light trapping especially in the wavelength range of 400–800 nm. This observed phenomenon of the pillar height dependent light trapping can be related to the increase in carrier recombination with the further increase of Si NP height. It also worth to note that as majority of the short-wavelength photons are absorbed in first 10 nm of Si or so, the most significant drop in EQE is witnessed at those short wavelengths for cells with the taller pillars, while there is no substantial change for the wavelengths >800 nm, since most of the long-wavelength photons are absorbed in the bulk of Si. All these indicate an effective surface passivation, especially the junction passivation, being inevitable to further advance the electrical performance of these NP-based hybrid solar cells.

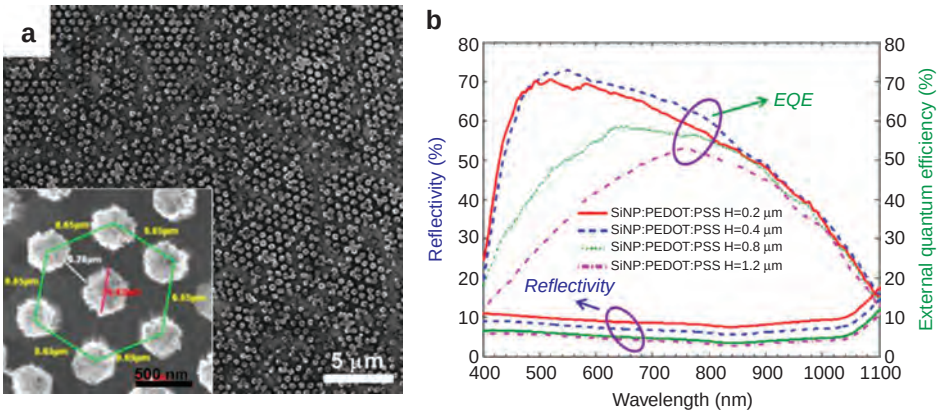

Fig. 5 (a) Top view SEM image of a Si NP array textured silicon surface; the inset shows the higher magnification image of the same sample, where it is possible to identify the hexagonal order of the NP array. (b) Reflectivity spectra and measured external quantum efficiency of the fabricated Si NP/PEDOT:PSS hybrid solar cells with different Si NP height. Reproduced from Ref. [9] with permission from The American Chemical Society.

Tapered nanostructures: nanopyramids, nanocones, and nanodomes

Along with NWAs and NPs, fine-designed nanostructures with the tapered geometry and shape, such as nanocones, nanopyramids and nandomes, etc, have illustrated superior antireflection properties due to their graded transition of the effective refractive index between the nanostructures and air [73–77]. Among these tapered nanostructures, nanocones (NCNs) have been considered as the optimal structure for light harvesting since their optical reflection can be significantly reduced over a broad range of wavelength through their smaller tip as compared with NWAs and NPs [78–80]. Wang et al. performed systematic simulation studies on the optical properties of silicon NCNs and contrasted them with those of NWAs [80]. NCN arrays are found to have the significantly enhanced solar absorption and efficiencies over NW arrays due to the reduced reflection from their smaller tip and reduced transmission from their larger circular base. Furthermore, these anti-reflection properties are found to be insensitive to the tip diameter, facilitating their fabrication for practical applications. This way, the optical absorption enhancement in amorphous Si NCs was experimentally investigated by Yi et al. [81]. The fabrication process of NCs is depicted in Fig. 6a–d. A monolayer of silica nanoparticles is used as an etch mask during a chlorine-based RIE process and either NWs or NCs can be obtained through controlling the process conditions because the etching rate of silica is much lower than that of amorphous Si. It could be found that in contrast with the amorphous film and NWs, a graded transition of the effective refractive index is observed for NCs due to the gradual shrinking of the diameter from the root to the top (Fig. 6e–g). Providing the perfect impedance matching between amorphous Si and air through the gradual reduction of the effective refractive index, NCs display the stronger absorption over a large range of wavelengths and angles of incidence (Fig. 6h–i). These excellent and omnidirectional light absorption characteristics can provide a higher integrated power generation over conventional planar structures; as a result, these amorphous Si NCs can offer a promising PV structure as both absorber and antireflection layers for the efficient solar cells.

Nanopyramid (NPM) is another kind of tapered nanostructure with the square base. This NPM structure can be obtained by the most common surface texturization technique through the anisotropic chemical etching of silicon in the alkaline solution [82, 83]. Mavrokefalos et al. demonstrated an inverted nanopyramid light-trapping scheme fabricated at wafer-scale via a low-cost wet etching process [84]. Commercial Si-on-insulator (SOI) substrates were selected with the desired Si and SiO_2 thickness. Then, hole arrays were patterned in negative photoresist on the top Si surface followed by the subsequent wet etching in the aqueous KOH solution to yield the inverted pyramid structure. KOH wet chemistry was utilized as it etched

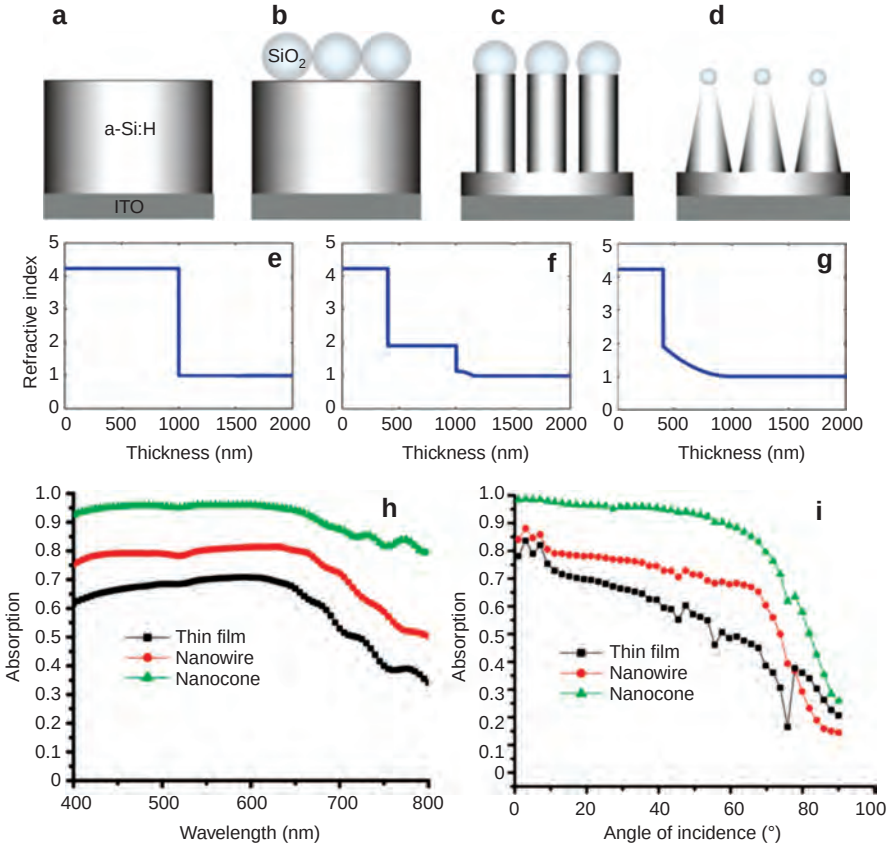

Fig. 6 (a–d) Schematic illustration of 1 μm thick amorphous Si deposited on the ITO-coated glass substrate, a monolayer of silica nanoparticles on top of the amorphous thin film, NW arrays and NC arrays. The effective refractive index profiles of the interfaces between air and (e) amorphous Si thin film, (f) 600 nm NW arrays, and (g) 600 nm NC arrays. (h) Measured absorption of samples with amorphous thin film, NW arrays and NC arrays as the top layer over a large range of wavelength at the normal incidence. (i) Measured angular dependent absorption of three samples at the wavelength of $\lambda = 488$ nm. Reproduced from Ref. [81] with permission from The American Chemical Society.

crystalline Si anisotropically along <100> crystal direction. The fabricated NPM structures are presented in Fig. 7a. Samples of varying ridge size yielded absorptance fluctuations that are most pronounced at short wavelengths [84]. Magnified SEM images display the separation between successive pyramids being about 100 nm with the fluctuation of 10 nm (Fig. 7a inset). These inverted pyramids exhibit an obvious optical absorption enhancement throughout the entire solar spectrum as compared with that of the flat film (Fig. 7b). Notably, the absorptance of this 10 μm thick Si layer with the inverted NPM structure is found to approach the Yablonovitch limit with the minimal angle dependence [85], confirming the effectiveness of trapping photons in NPMs.

Similarly, nanodomes (NDMs) combine many nanophotonic effects in effectively reducing the optical reflection and enhanced absorption over a broad spectral range. Zhu et al. have illustrated nanodome amorphous Si solar cells with the efficient light management fabricated on NCN substrates after the deposition of solar cell layers, as shown in Fig. 8a–c [86]. These NDM devices consist of only a 280 nm thick hydrogenated amorphous silicon absorber layer, which can provide the much higher absorption than flat film devices over the entire spectrum and a large range of incident angles (Fig. 8d–f). This anti-reflection effect mainly comes from the tapered shape of NDM structures with the better effective reflective index matching with air, particularly coupling light into the amorphous layer with suppressed reflection as well as scattering light along the in-plane dimension. This scattering can increase the light traveling path by trapping photons. Notably, there is a significant interference oscillations appeared in the flat film devices

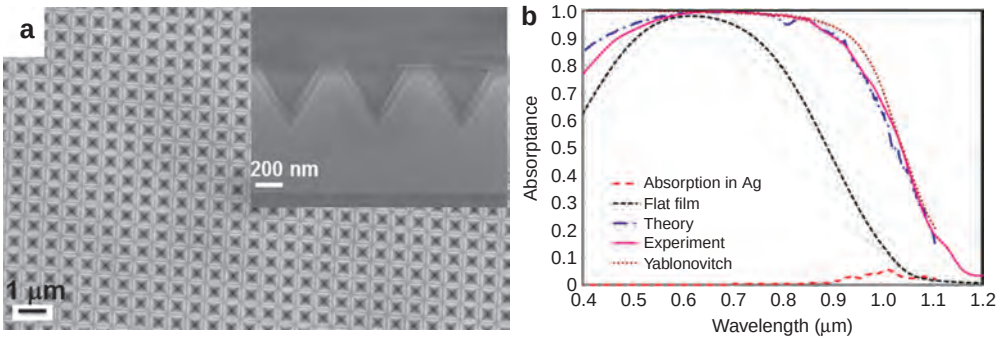

Fig. 7 (a) Top view SEM images of the 10 μm thick crystalline Si film illustrating the patterned inverted nanopyramids on a 700 nm period. A 90 nm SiN_x layer is deposited on the inverted pyramids and a SiO_2 (1 μm) and a silver (200 nm) layer are at the backside of the c-Si film. The top left inset is the close-up cross-sectional SEM picture of the same device. (b) Comparison of the theoretical and experimental absorptance spectra, the Yablonovitch limit corresponding to the c-Si thickness and the calculated absorptance in the Ag layer for the top Si film thicknesses of 10 μm. Reproduced from Ref. [84] with permission from The American Chemical Society.

for the long wavelength above 550 nm, while NDM devices still show relatively flat broadband adsorption for the long wavelength region, indicating the NDM structure is feasible for thin film solar cells with only submicrometer thick absorber layers, attributed to the reduced reflection and avoiding interference oscillations for longer wavelengths. Also, the NDM structure is in principle not restricted to any particular material system and its fabrication is compatible with most post-solar manufacturing. Therefore, all these can initiate many exciting opportunities for an assortment of PV devices to further improve efficiency and minimize the materials usage.

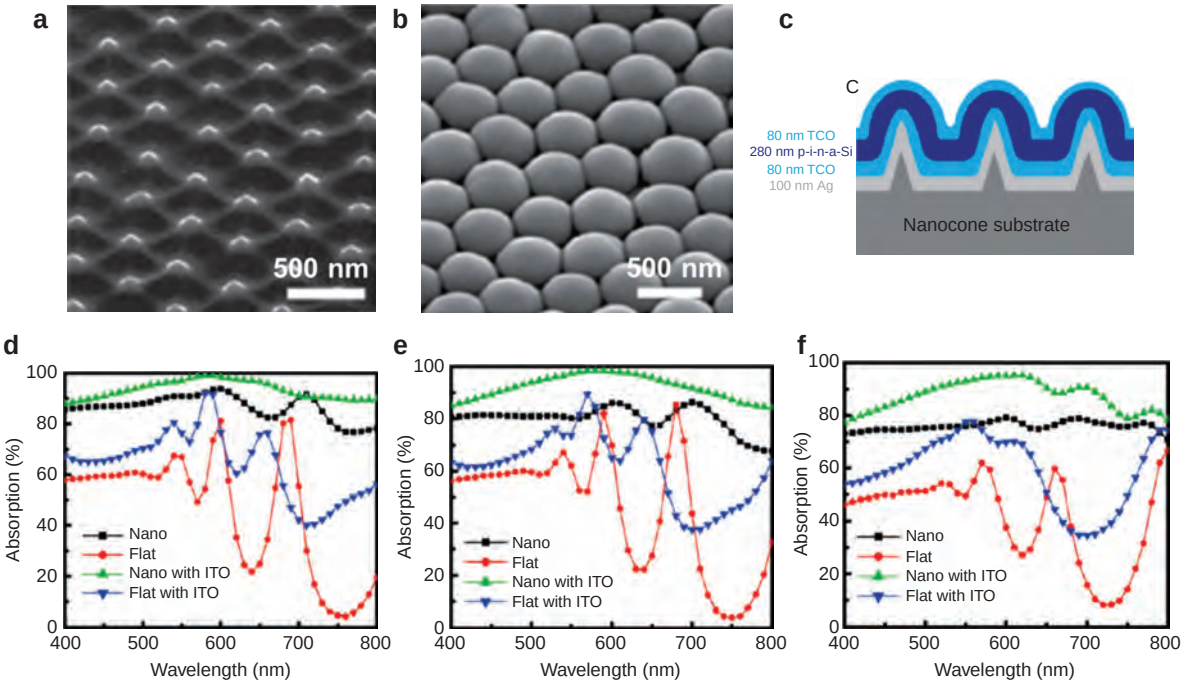

Fig. 8 SEM images with a 45° tilt angle of (a) nanocone quartz substrates and (b) amorphous Si nanodome solar cells after the deposition of multilayers of materials on nanocones. (c) Schematics of the cross-sectional structure of nanodome solar cells. (d–f) Light absorption measurement of nanodomes and flat substrates with and without ITO. (d) Integrating sphere measurement results of absorption under the normal incidence, (e) 30° angle of incidence, (f) 60° angle of incidence. Reproduced from Ref. [86] with permission from The American Chemical Society.

Nanoholes and nanowells

Besides vertically aligned "positive" nanostructures discussed above, "negative" nanostructures such as nanoholes (NHs) and nanowells (NWs) also demonstrate the impressive light management property. Han et al. investigated silicon NH arrays as light absorbing structures for photovoltaics via the simulation and compared them to that of NR arrays [87]. Figure 9a–b show the schematic illustrations of NH and NR arrays. The absorption spectra for NH and NR arrays with the structure thickness of 1.193 mm and 2.33 μm were calculated and shown in Fig. 9c. Results show that the absorption of NH array is higher than that of NR arrays at the wavelength <750 nm in regardless of the structure thickness. While at the long wavelength region (750 nm < λ < 1 μm), the thin NH array (1.193 μm thickness) can absorb more strongly than the NR array, indicating that the light trapping in the small volume is more efficient for the NH array. Experimentally, MacEtch processes have also been employed to fabricate these "negative" nanostructures as anti-reflection layers. For example, nanopore-type "black" Si has been achieved by one-step Ag-assisted chemical etching involving HF and H_2O_2 solution [88]. Lower reflectivity can be compromised between the sufficient Ag catalyst to create large numbers of nanopores (~100 nm in diameters) on Si surface and the excessive Ag which would induce the deeply etched channels creating potential short-circuit in the subsequent solar cell fabrication. By controlling the etching condition, the lowest relative effective reflectivity of 0.17 % over a wide wavelength range of 300–1000 nm is realized for the nanopore Si made of $[Ag^+]$ = 50 mM with 20 min etching and HF: H_2O_2: H_2O ratio of 1:5:2. The simplicity and effectiveness of this structure can make such processing easily scalable for industrial applications.

Applications in solar cells

For photovoltaic applications, 3D nanostructures cannot only lead to improved photon harvesting properties utilizing the light trapping mechanism, but also enhance the photo-carrier collection efficiency due to the shorted diffusion length in p-n junctions [89–91]. Generally, there are two main configurations of p–n junction, i.e., radial (core-shell) junctions and axial junctions. The radial junction can enhance the carrier collection efficiency as compared to the axial junctions, as long as the radii of the nanostructures are much smaller than the minority diffusion length [89, 92]. In radial p–n structures, the separation and collection of photo-generated carriers take place in the radial direction and such geometry provides short travel distances of photo-excited minority carriers to the collection electrodes, leading to the improved carrier-collection efficiency [18, 32, 93]. Furthermore, the radial geometry of p–n junction in 3D nanostructures permits the use of lower-quality silicon with shorter minority-carrier diffusion length. For example, arrays of vertical rods with

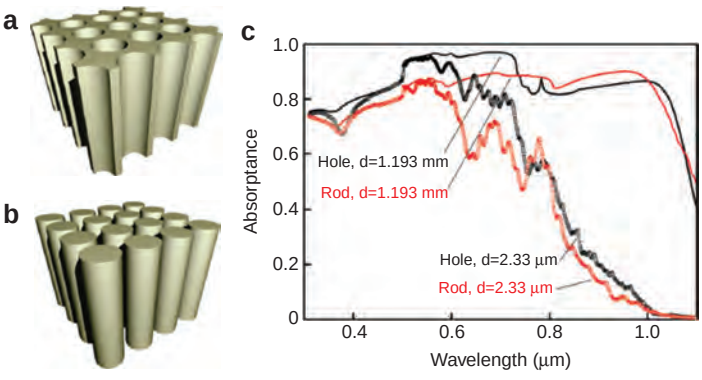

Fig. 9 (a) Schematic illustrations of the nanohole and (b) nanorod arrays. (c) Calculated absorptance spectra for the nanohole and the nanorod array structures when the thickness d is 2.33 μm and 1.193 mm. Reproduced from Ref. [87] with permission from The American Chemical Society.

a core-shell p–n junction structure have been theoretically shown to be capable of improving photo-generated carrier collection for poor-quality material with short minority carrier diffusion lengths, as reported by B. M. Kayes et al. [15], indicating a high tolerance of material defects for PVs [91].

Regardless of the above-mentioned potential advantages inspired by the radial p-n junction with excellent light trapping properties, most studies show that the PV performance of nanostructured solar cells is not satisfying in spite of the strong optical enhancement [9, 16–18]. The degradation of device performance is mostly attributed to the high recombination effect caused by high-density surface defects as well as the large surface area in these high-aspect-ratio nanostructures [67, 93, 94]. A competition between the improved absorption and increased surface recombination was observed and investigated by Garnett et al., by changing the silicon film thickness and nanowire length [67]. Figure 10a and b show the photovoltaic performance of 5 μm tall NW as well as planar control solar cells under AM 1.5G illumination while devices with different silicon absorber thicknesses were discussed. It could be seen that NW cell fabricated from an 8 μm thin silicon absorber gave a 4 % higher Jsc versus the planar control cell, indicating that the light-trapping effects dominate for very thin absorbing layers. While for NW cell using the 20 μm silicon absorbing layer, it had a 14 % lower Jsc than the planar control solar cell, because the recombination effect is more important for thicker cells that already absorb a large fraction of the incident light. In order to further explore the optical trapping advantages and recombination disadvantages of nanowire arrays, Fig. 10c depicts the photovoltaic characteristics for 8 μm cells fabricated with various nanowire lengths, leading to different roughness factors. The roughness factor (RF) is defined as the actual surface area of the structure divided by the geometric area (e.g., RF of a planar cell is 1) [67]. The trends of Voc, FF, and Jsc show that the increased surface and junction areas lead to the enhancement of both recombination (i.e., lower Voc and FF) and light trapping effect (i.e., higher Jsc). It also appears that the light-trapping effect dominates over the recombination effect for this Si absorber thickness, as the Jsc continues to increase with higher RF.

To suppress the recombination effect, it would be critical to take proper surface treatments or design improved nanoarray geometries that allow for lower roughness factors without sacrificing the light trapping. Deposition of surface passivation layers can effectively reduce the surface recombination through the reduction of interface traps and the implementation of a field-effect passivation [95]. Chen et al. demonstrated a highly efficient nanotextured black silicon solar cell with a n^+ emitter/p base structure passivated by the Al_2O_3 layer through the atomic layer deposition (ALD) (shown in Fig. 11a) [19]. The nanotextured black silicon wafer covered with the 11 nm thick Al_2O_3 layer exhibited a very low total reflectance of ~1.5 % in a broad spectrum from 400 to 800 nm, as presented in Fig. 11b. Figure 11c gives the illuminated current-voltage (I–V) curves of the cells with and without the Al_2O_3 passivation layer. By comparing cell 1 (without passivation layer) and cell 2 (with Al_2O_3 passivation layer), one could find that Jsc and η were enhanced ~5.5 % and 7.3 % by the as-deposited Al_2O_3 surface passivation layer. Thus the efficiency enhancement can be mainly attributed to the increase of Jsc due to the suppression of surface recombination by the as-deposited passivation layer.

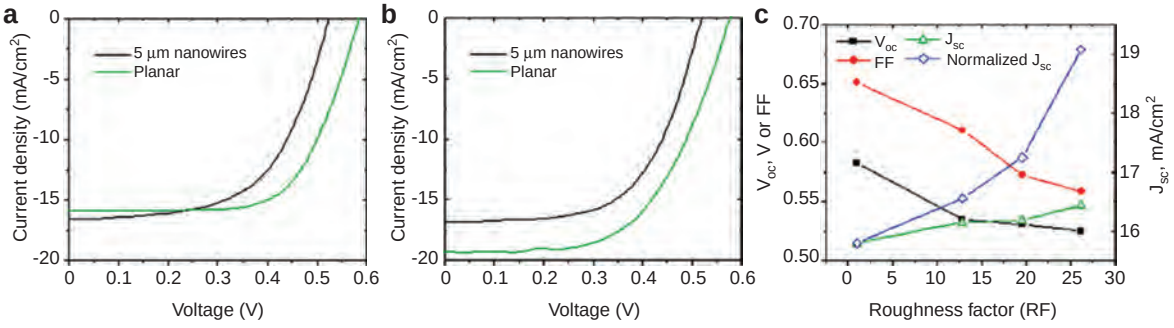

Fig. 10 (a) Photovoltaic performance of 5 μm nanowire and planar control solar cells fabricated from (a) 8 μm and (b) 20 μm thin silicon absorbers. (c) Photovoltaic response as a function of roughness factor. Reproduced from Ref. [67] with permission from The American Chemical Society.

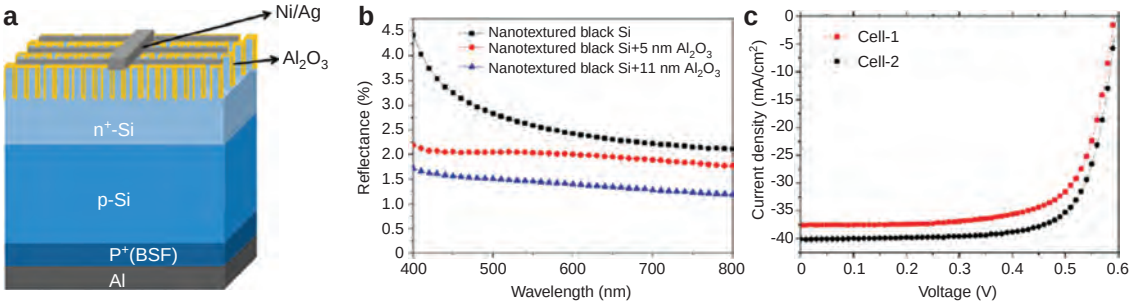

Fig. 11 (a) Schematic diagram of the nanotextured black silicon solar cell with an n+ emitter/p base structure. (b) Total reflectance spectra of the nanotextured black silicon wafer with and without the Al_2O_3 layers. (c) Illuminated I–V characteristics of the cells with (cell 2) and without (cell 1) 11 nm Al_2O_3 passivation layer. Reproduced from Ref. [19] with permission from The American Chemical Society.

In addition to Al_2O_3, several materials have demonstrated with the excellent surface passivation effect, such as silicon oxide and hydrogenated silicon nitride layer manufactured by plasma enhanced chemical vapor deposition (PECVD) [20, 21]. Also, the combination of PECVD based silicon oxide and silicon nitride has been proved to be a very promising approach for surface passivation, which has been successfully integrated in many cell structures [22, 23].

Specifically, the surface recombination can be reduced by the deposition of a surface passivation layer because of the following reasons: (1) the decrease in interfacial state density, i.e., the so-called chemical passivation, and (2) the reduction in minority carrier concentration near the interface by the built-in electric field, which is referred to the field-effect passivation [96]. The built-in electric field established by the appropriate fixed charge in the surface passivation layer, can give rise to repelling of minority carriers away from the interface, leading to a lower surface recombination rate. Instead of nanostructured silicon solar cells, other semiconductor solar cells also get benefits from this surface passivation. Mariani et al. reported that in-situ passivation treatment could dramatically improve the external quantum efficiency and total power conversion efficiency of GaAs-based nanopillar array solar cells [97]. Holm et al. [98] also demonstrated that the surface passivation plays a crucial role in the GaAsP single nanowire solar cells, as summarized in Table 1.

Besides, a chemical polishing etching (CPE) treatment has been found as another effective way to reduce the surface recombination in high-aspect-ratio nanostructures by decreasing the surface defects and control the final morphologies of the as-made structures, as reported by Wang et al. [18] In their work, large-area uniform hierarchical structures combining NPMs and NWs were obtained by the metal-assisted chemical etching. A CPE solution which is the mixture of nitric acid (HNO_3) and hydrofluoric acid (HF) was applied to the hierarchical structures leading to an atomically smooth and contamination-free surface (Fig. 12a–c). Reflectance spectra of the hierarchical structures with different CPE durations and J-V characteristics of Si

Table 1 Summary of the current status of solar cell efficiency based on three-dimensional silicon, compound semiconductor and hybrid nanostructures.

Group	Solar cell type	PCE (%)
Miin-Jang Chen et al. [19]	Nanowire-based silicon solar cells	18.2
Yi Cui et al. [86]	Nanodome-based silicon solar cells	5.9
Futing Yi et al. [72]	Nanopillar-based silicon solar cells	14.83
Jr-Hau He et al. [18]	Hierarchical structure-based silicon solar cells (pyramids + nanowires)	15.14
Pushpa Raj Pudasaini et al. [9]	Nanopillar-based hybrid Si/PEDOT:PSS solar cells	9.65
Yi Cui et al. [79]	Nanocone-based hybrid Si/PEDOT:PSS solar cells	11.1
Huffaker DL. et al. [97]	GaAs nanopillar-array solar cells	6.63
Jeppe V. Holm et al. [98]	GaAsP single-nanowire solar cells	10.2

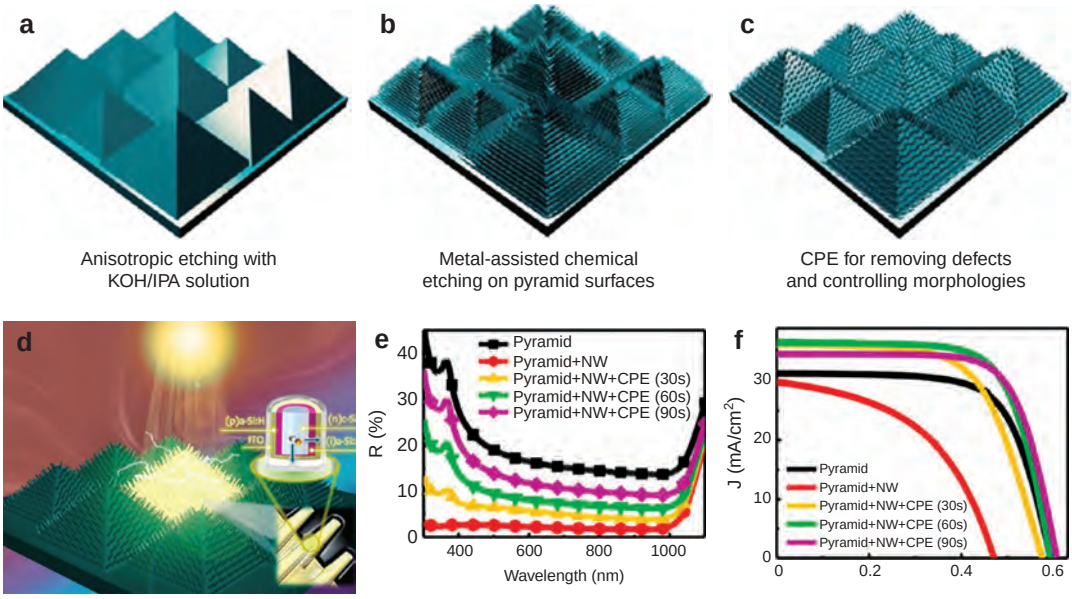

Fig. 12 (a–c) Schematics of the experimental procedures. (d) The corresponding solar cell structure. (e) Total reflectance spectra of hierarchical structures with different CPE durations over the wavelength regions of 300–1100 nm. (f) J–V characteristics the solar cells with different structures under AM 1.5G illumination. Reproduced from Ref. [18] with permission from The American Chemical Society.

heterojunction solar cells (Fig. 12d) are shown in Fig. 12e and f, respectively. The lowest reflectance could be observed in the pyramid-NW hierarchical structure without CPE treatment due to its excellent light trapping property, while poor PV performance is demonstrated which is attributed to high-density carrier trapping centers. After treated by CPE, all the structures exhibit higher photovoltaic conversion efficiencies even though there is a decrease in the reflectance due to the formation of relatively polished surfaces. Especially, Jsc of the solar cell with hierarchical structures is increased from 29.83 to 36.58 mA/cm^2 after 60 s CPE, owing to the smoother surface and the decrease in junction area. Nevertheless, Jsc decreases as the CPE time prolongs further, demonstrating an overall geometrical consideration of both light trapping and recombination effect should be emphasized to yield the best photovoltaic properties for the hierarchical structures based solar cell. More importantly, this unique cell structure also illustrates the omnidirectional PV properties, exhibiting the daily generated power enhancement of 44.2 % as compared to conventional micropyramid control cells and demonstrating the technological potency of 3D hierarchical structures for the next-generation solar cells [18].

Furthermore, thin-film solar cells are presently considered as another promising route to lower the material and processing cost of photovoltaics [99]. However, the PV performance of thin-film solar cells is significantly affected by thinning down the active layer and the corresponding light trapping becomes an important limiting factor. By combining low-cost thin-film solar cells with nanostructured surface texturization, the light harvesting properties could be improved. Nanocone structures with excellent light trapping properties were employed in the hybrid Si thin film solar cells, as reported by Jeong et al. [79]. With a very thin active material and inexpensive processing steps, hybrid Si nanocone/polymer solar cells could demonstrate high power conversion efficiency above 11 %, demonstrating an economically viable alternative energy solution (Table 1). In addition to the surface texturization, recent research has also shown that integrating plasmonic nanostructures is an alternative feasible approach to enhance the light trapping properties for thin-film solar cells by using metallic nanoparticles to couple light into the underlying optical modes of the semiconductor [100]. In order to enhance the optical absorption in the solar spectrum, tuning the surface plasmon resonance can be utilized. Specifically, the excitation of surface plasmons can be characterized by the strong scattering as well as the enhancement of electric field around the surrounding area of nanoparticles [101]. Photocurrent enhancements

have been reported from both inorganic, organic solar cells and hybrid inorganic-organic devices such as dye sensitized solar cells [102–104]. For example, Matheu et al. [104] have described an increase in the power conversion efficiency of 2.8 % and 8.8 % from Si-based devices using 100 nm Au colloidal particles and 150 nm silica particles, respectively. The similar approach has also been applied to GaAs thin-film solar cells with an 8 % increase in the short-circuit current density utilizing 110 nm silver particles [105]. Based on all these results, the potential of incorporating plasmonics into solar cell structures looks very encouraging. In any case, special attention must be paid to the density of nanoparticles deposited on the top cell surface in order to avoid the shadowing effect, which would degrade the corresponding light absorption if not properly optimized [99].

Conclusion

In this review, the controllable fabrication of three-dimensional silicon nanostructures has been summarized. Among various fabrication techniques, MacEtch is a more flexible and promising method to fabricate high-aspect-ratio nanostructures for photovoltaic applications because there is no surface damage and metal contamination caused in the fabrication process. Meanwhile, the light trapping properties of several major categories of silicon nanostructures are systematically compared and it is revealed that nanostructures with diverse configurations have demonstrated excellent but unique photon management properties. Particularly, nanocone (NCN) structure has been considered as one of the optimal structures for light harvesting due to their reduced reflection over a broad range of wavelengths through a graded effective refractive index, and their small tips also contribute to a reduced reflectance compared with other nanostructures. Even though these nanostructures with radial p–n junction can demonstrate improved photon harvesting properties and enhanced photo-carrier collection efficiencies, the photovoltaic performance of nanostructure-based devices is still significantly limited by the high recombination effect coming from high-density surface defects in nanostructures with the large surface area. In this regard, various approaches have been discussed to reduce the surface recombination in these high-aspect-ratio nanostructures, such as depositing passivation layers as well as chemical polishing etching treatment. All in all, a concurrent improvement in both electrical and optical characteristics of the radial junction Si nanostructures is the most important issue for putting high-efficiency nanostructured based solar cells into practice.

Acknowledgments: This research was financially supported by the City University of Hong Kong (Project no. 9667054).

References

[1] D. Ginley, M. Green, R. Collins. *MRS Bull.* **33**, 355–373 (2008).
[2] A. Hochbaum, P. Yang. *Chem. Rev.* **110**, 527–546 (2010).
[3] M. Law, J. Goldberger, P. Yang. *Annu. Rev. Mater. Res.* **34**, 83–122 (2004).
[4] B. Tian, T. J. Kempa, C. M. Lieber. *Chem. Soc. Rev.* **38**, 16–24 (2009).
[5] Z. Y. Fan, D. J. Ruebusch, A. A. Rathore, R. Kapadia, O. Ergen, P. W. Lue, A. Javey. *Nano Res.* **2**, 829–843 (2009).
[6] K. Yu, J. Chen. *Nanoscale Res. Lett.* **4**, 1–10 (2008).
[7] N. S. Lewis, D. G. Nocera. *Proc. Natl. Acad. Sci. USA* **103**, 15729–15735 (2006).
[8] L. Dupré, D. Buttard, P. Gentile, N. Pauc, Amit Solanki. *Energy Procedia* **10**, 33–37 (2011).
[9] P. R. Pudasaini, F. Ruiz-Zepeda, M. Sharma, D. Elam, A. Ponce, A. A. Ayon. *ACS Appl. Mater. Interfaces* **5**, 9620–9627 (2013).
[10] R. Yu, Q. Lin, S. F. Leung, Z. Fan. *Nano Energy* **1**, 57–72 (2012).
[11] Y. Long, M. Yu, B. Sun, C. Gu and Z. Fan. *Chem. Soc. Rev.* **41**, 4560–4580 (2012).
[12] Z. Fan, A. Javey. *Nat. Mater.* **7**, 835–836 (2008).
[13] M. D. Kelzenberg, S. W. Boettcher, J. A. Petykiewicz, D. B. Turner-Evans, M. C. Putnam, E. L. Warren, J. M. Spurgeon, R. M. Briggs, N. S. Lewis, H. A. Atwater. *Nat. Mater.* 239–244 (2010).
[14] W. R. Wei, M. L. Tsai, S. T. Ho, S. H. Tai, C. R. Ho, S. H. Tsai, C. W. Liu, R. J. Chung, J. H. He. *Nano Lett.* **13**, 3658–3663 (2013).
[15] B. M. Kayes, H. A. Atwater, N. S. Lewis. *J. Appl. Phys.* **97**, 114302–114312 (2005).
[16] G. Oki, G. Supratik. *Sol. Energy Mater. Sol. Cells* **93**, 1388–1393 (2009).

[17] S. K. Srivastavaa, D. Kumara, P. K. Singha, M. Kara, V. Kumara, M. Husain. *Sol. Energy Mater. Sol. Cells* **94**, 1506–1511 (2010).
[18] H. P. Wang, T. Y. Lin, C.W. Hsu, M. L. Tsai, C. H. Huang, W. R. Wei, M. Y. Huang, Y. J. Chien, P. C. Yang, C. W. Liu, L. J. Chou, J. H. He. *ACS Nano* **7**, 9325–9335 (2013).
[19] W. C. Wang, C. W. Lin, H. J. Chen, C. W. Chang, J. J. Huang, M. J. Yang, B. Tjahjono, J.J. Huang, W. C. Hsu, M. J. Chen. *ACS Appl. Mater. Interfaces* **5**, 9752–9759 (2013).
[20] J. M. Kopfer, S. Keipert-Colberg, D. Borchert. *Thin Solid Films* **519**, 6525–6529 (2011).
[21] G. Dingemans, W. M. M. Kessels. *J. Vac. Sci. Technol. A* **30**, 040802 (2012).
[22] J. Schmidt, M. Kerr, A. Cuevas. *Semicond. Sci. Technol.* **16**, 164–170 (2001).
[23] O. Schultz, M. Hofmann, S. W. Glunz, G. P. Willeke. *Proceedings of the 31st IEEE Photovoltaic Specialists Conference,* 872–876 (2005).
[24] R. S. Wagner, W. E. Ellis. *Appl. Phys. Lett.* **4**, 89 (1964).
[25] Y. Wu, P. Yang. *J. Am. Chem. Soc.* **123**, 3165–3166 (2001).
[26] Y. Wang, V. Schmidt, S. Senz U. Gösele. *Nat. Nanotechnol.* **1**, 186–189 (2006).
[27] J. J. Hou, N. Han, F. Y. Wang, F. Xiu, S. P. Yip, A. T. Hui, T. F. Hung, J. C. Ho. *ACS Nano* **6**, 3624–3630 (2012).
[28] N. Han, F. Y. Wang, A. T. Hui, J. J. Hou, G. C. Shan, F. Xiu, T. F. Hung, J. C. Ho. *Nanotechnology* **22**, 285607 (2011).
[29] T. Hanrath, B. A. Korgel. *J. Am. Chem. Soc.* **124**, 1424–1429 (2002).
[30] W. I. Park, G. Zheng, X. Jiang, B. Tian, C. M. Lieber. *Nano Lett.* **8**, 3004–3009 (2008).
[31] A. Martí, N. López, E. Antolín, E. Cánovas, C. Stanley, C. Farmer, L. Cuadra, *Solid Films* **511**, 638–644 (2006).
[32] L. Tsakalakos, J. Balch, J. Fronheiser, B. A. Korevaar, O. Sulima, J. Rand. *Appl. Phys. Lett.* **91**, 233117 (2007).
[33] Z. W. Pan, Z. R. Dai, L. Xu, S. T. Lee, Z. L. Wang. *J. Phys. Chem. B* **105**, 2507–2514 (2001).
[34] S. J. Kwon. *J. Phys. Chem. B* **110**, 3876–3882 (2006).
[35] W. S. Shi, Y. F. Z. N. Wang, C. S. Lee, S. T. Lee. *Appl. Phys. Lett.* **78**, 3304–3306 (2001).
[36] Y. Zhang, H. Jia, D. J. Yu. *Phys. D: Appl. Phys.* **37**, 413–415 (2004).
[37] M. J. Bierman, Y. K. A. Lau, A. V. Kvit, A. L. Schmitt, S. Jin. *Science* **320**, 1060–1063 (2008).
[38] P. J. Poole, L. J. efebvre, J. Fraser. *Appl. Phys. Lett.* **83**, 2055– 2057 (2003).
[39] J. Noborisaka, J. Motohisa, T. Fukui. *Appl. Phys. Lett.* **86**, 213102 (2005).
[40] N. Wang, Y. H. Tang, Y. F. Zhang, C. S. Lee, I. Bello, S. T. Lee. *Chem. Phys. Lett.* **299**, 237–242 (1999).
[41] R. Q. Zhang, Y. Lifshitz, S. T. Lee. *Adv. Mater.* **15**, 635–640 (2003).
[42] C. P. Li, C. S. Lee, X. L. Ma, N. Wang, R. Q. Zhang, S. T. Lee. *Adv. Mater.* **15**, 607–609 (2003).
[43] Y. F. Zhang, Y. H. Tang, N. Wang, D. P. Yu, C. S. Lee, I. Bello, S. T. Lee. *Appl. Phys. Lett.* **72**, 1835 (1998).
[44] N. Wang, Y. F. Zhang, Y. H. Tang, C. S. Lee, S. T. Lee. *Phys. Rev. B* **58**, R16 024 (1998).
[45] S. T. Lee, Y. F. Zhang, N. Wang, Y. H. Tang, I. Bello, C. S. Lee, Y. W. Chung. *J. Mater. Res.* **14**, 4503 (1999).
[46] B. S. Kim, T. W. Koo, J. H. Lee, D. S. Kim, Y. C. Jung, S. W. Hwang, B. L. Choi, E. K. Lee, J. M. Kim, D. Whang. *Nano Lett.* **9**, 864–869 (2009).
[47] Y. Huang, X. Huan, C. M. Lieber. *Small* **1**, 142 (2005).
[48] S. H. G. Teo, A. Q. Liu, G. L. Sia, C. Lu. *Int. J. Nanosci.* **4**, 567–574 (2005).
[49] L. Sainiemi, H. Keskinen, M. Aromaa, L. Luosujarvi, K. Grigoras, T. Kotiaho, J. M. Makela, S. Franssila. *Nanotechnology* **18**, 505303–505310 (2007).
[50] K. J. Morton, G. Nieberg, S. Bai, S. Y. Chou. *Nanotechnology* **19**, 345301 (2008).
[51] F. Lärmer, A. Schilp. U.S. Patent 4241 045 (1996).
[52] W. Lang. *Mater. Sci. Eng.* **1**, R. 17 (1996).
[53] H. Rhee, H. Kwon, C. K. Kim, H. J. Kim, J. Yoo, Y. W. Kim. *J. Vac. Sci. Technol. B* **26**, 576 (2008).
[54] Y. Q. Fu, A. Colli, A. Fasoli, J. K. Luo, A. J. Flewitt, A. C. Ferrari, W. I. Milne. *J. Vac. Sci. Technol.* B **2**, 1520–1526 (2009).
[55] G. S. Oehrlein, S. M. Rossnagel, (Ed.), *Noyes*, Park Ridge, NJ, pp. 196 (1990).
[56] X. L. Li. *Curr. Opin. Solid State Mater. Sci.* **16**, 71–81 (2012).
[57] X. L. Li, P. W. Bohn. *Appl. Phys. Lett.* **77**, 2572–2574 (2000).
[58] Z. Huang, N. Geyer, P.Werner, J. de Boor, U. Gosele. *Adv. Mater.* **23**, 285–308 (2011).
[59] H. Lin, H. Y. Cheung, F. Xiu, F. Y. Wang, S. P. Yip, N. Han, T. F. Hung, J. Zhou, J. C. Ho, C. Y. Wong. *J. Mater. Chem. A* **1**, 9942–9946 (2013).
[60] L. Schubert, P. Werner, N. D. Zakharov, G. Gerth, F. M. Kolb, L. Long, U. Gosele, T. Y. Tan. *Appl. Phys. Lett.* **84**, 4968 (2004).
[61] W. Chern, K. Hsu, I. S. Chun, B. P. D. Azeredo, N. Ahmed, K. H. Kim, J. M. Zuo, N. Fang, P. Ferreira, X. Li. *Nano Lett.* **10**, 1582–1588 (2010).
[62] X. H. Li, R. Song, Y. K. Ee, P. Kumnorkaew, J. F. Gilchrist, N. Tansu. *IEEE Photon*. J. **3**, 489–499 (2011).
[63] Y. K. Ee, P. Kumnorkaew, R. A. Arif, H. Tong, H. Zhao, J. F. Gilchrist, N. Tansu. *IEEE J. Sel. Topics Quantum Electron.* **4**, 1218–1225 (2009).
[64] I. S. Chun, E. K. Chow, X. Li. *Appl. Phys. Lett.* **92**, 191113–191115 (2008).
[65] J. A. Rogers, R. G. Nuzzo. *Mater. Today* **8**, 50–56 (2005).
[66] X. H. Yang, F. G. Zeng, X. J. Li. *Mater. Sci. Semicond. Process.* **16**, 10 (2013).
[67] E. Garnett, P. Yang. *Nano Lett.* **10**, 1082–1087 (2010).

[68] B. Tian, X. Zheng, T.J. Kempa, Y. Fang, N. Yu, G. Yu, J. Huang, C.M. Lieber. *Nature* **449**, 885–889 (2007).
[69] S.W. Boettcher, J. M. Spurgeon, M. C. Putnam, E. L. Warren, D. B. Turner-Evans, M. D. Kelzenberg, J. R. Maiolo, H. A. Atwater, N. S. Lewis. *Science* **327**, 185 (2010).
[70] T. J. Kempa, B. Tian, D. R. Kim, J. Hu, X. Zheng, C. M. Lieber. *Nano Lett.* **8**, 3456–3460 (2008).
[71] O. Gunawan, K. Wang, B. Fallahazad, Y. Zhang, E. Tutuc, S. Guha. *Prog. Photovolt: Res. Appl.* **19**, 307–312 (2011).
[72] J. Liu, M. Ashmkhan, X. Zhang, G. Dong, Y. Liao, B. Wang, T. Zhang, F. Yi. *Energy Technol.* **1**, 139–143 (2013).
[73] Y. F. Huang, S. Chattopadhyay, Y.J. Jen, C. Y. Peng, T. A. Liu, Y. K. Hsu, C. L. Pan, H. C. Lo, C. H. Hsu, Y. H. Chang, C. S. Lee, K. H. Chen, L. C. Chen. *Nat. Nanotechnol.* **2**, 770–774 (2007).
[74] Y. J. Lee, D. S. Ruby, D. W. Peters, B. B. McKenzie, J. W. P. Hsu. *Nano Lett.* **8**, 1501–1505 (2008).
[75] T. Lohmuller, M. Helgert, M. Sundermann, R. Brunner, J. P. Spatz. *Nano Lett.* **8**, 1429–1433 (2008).
[76] J. Zhu, Z. Yu, G. F. Burkhard, C. M. Hsu, S. T. Connor, Y. Xu, Q. Wang, M. McGehee, S. Fan, Y. Cui. *Nano Lett.* **9**, 279– 392 (2009).
[77] Z. Yu, H. Gao, H. Wu, H. Ge, S. Y. Chou. *J. Vac. Sci. Technol. B* **21**, 3974–3977 (2003).
[78] K. X. Wang, Z. Yu, V. Liu, Y. Cui, S. Fan. *Nano Lett.* **12**, 1616–1619 (2012).
[79] S. Jeong, E. C. Garnett, S. Wang, Z. Yu, S. Fan, M. L. Brongersma, M. D. McGehee, Y. Cui. *Nano Lett.* **12**, 2971–2976 (2012).
[80] B. M. Wang, P. W. Leu. *Nanotechnology* **23**, 194003 (2012).
[81] Y. Cui. *Nano Lett.* **91**, 279–282 (2009).
[82] N. Marrero, B. Gonzalez-Diaz, R. Guerrero-Lemus. *Sol. Energy Mater. Sol. Cells* **91**, 1943–1947 (2007).
[83] X. S. Hua, Y. J. Zhang, H. W. Wang. *Sol. Energy Mater. Sol. Cells* **94**, 258–262 (2010).
[84] A. Mavrokefalos, S. E. Han, S. Yerci, M. S. Branham, G. Chen. *Nano Lett.* **12**, 2792–2796 (2012).
[85] E. J. Yablonovitch. *Opt. Soc. Am.* **72**, 899–907 (1987).
[86] J. Zhu, C. M. Hsu, Z. F. Yu, S. H. Fan, Y. Cui. *Nano Lett.* **10**, 1979–1984 (2010).
[87] S. E. Han, G. Chen. *Nano Lett.* **10**, 1012–1015 (2010).
[88] Y. T. Lu, A. R. Barron. *PCCP* **15**, 9862 (2013).
[89] S. H. Tsai, H. C. Chang, H. H. Wang, S. Y. Chen, C. A. Lin, S. A. Chen, Y. L. Chueh, J. H. He. *ACS Nano* **5**, 9501–9510 (2011).
[90] H. C. Chang, K. Y. Lai, Y. A. Dai, H. H. Wang, C. A. Lin, J. H. He. *Energy Environ. Sci.* **4**, 2863–2869 (2011).
[91] K. Q. Peng, S. T. Lee. *Adv. Mater.* **23**, 198–215 (2011).
[92] E. C. Garnett, M. L. Brongersma, Y. Cui, M. D. McGehee. *Annu. Rev. Mater. Res.* **41**, 269–295 (2011).
[93] E. C. Garnett, P. Yang. *J. Am. Chem. Soc.* **130**, 9224–9225 (2008).
[94] M. M. Adachi, M. P. Anantram, K. S. Karim. *Sci. Rep* **3**, 1–6 (2013).
[95] A.G. Aberle. *Prog. Photovolt Res. Appl.* **8**, 473 (2000).
[96] B. Hoex, J. J. H. Gielis, M. C. M. van de Sanden, W. M. M. Kessels. *J. Appl. Phys.* **104**, 113703 (2008).
[97] G. Mariani, A. C. Scofield, C. H. Hung, D. L. Huffaker. *Nat. Commun.* **4**, 1497 (2013).
[98] J. V. Holm, H. I. Jørgensen, P. Krogstrup, J. Nygaŕd, H. Liu, *M.* Aagesen. *Nat. Commun.* **4**, 1498 (2013).
[99] V. E. Ferry, J. N. Munday, H. A. Atwater. *Adv. Mater.* **22**, 4794–4808 (2010).
[100] H. A. Atwater, A. Polman. *Nat. Mater.* **9**, 205 (2010).
[101] S. Pillai, M.A. Green. *Solar Energy Materials & Solar Cells* **94**, 1481–1486 (2010).
[102] H. R. Stuart, D. G. Hall. *Appl. Phys. Lett.* **73**, 3815 (1998).
[103] V. E. Ferry, M. A. Verschuuren, H. B. T. Li, R. E. I. Schropp, H. A. Atwater, A. Polman. *Appl. Phys. Lett.* **95**, 183503 (2009).
[104] P. Matheu, S. H. Lim, D. Derkacs, C. McPheeters, E. T. Yu. *Appl. Phys. Lett.* **93**, 113108-1–113108-3 (2008).
[105] K. Nakayama, K. Tanabe, H. A. Atwater. *Appl. Phys. Lett.* **93**, 121904-1– 121904-3 (2008).